HHS Public Access

Author manuscript

Hepatology. Author manuscript; available in PMC 2022 October 01.

Published in final edited form as:

Hepatology. 2022 October ; 76(4): 1090–1104. doi:10.1002/hep.32363.

Zac1 and the Imprinted Gene Network program juvenile NAFLD in response to maternal metabolic syndrome

Marine Baptissart[1], **Christine M. Bradish**[1], **Brie S. Jones**[1], **Evan Walsh**[1], **Jesse Tehrani**[1], **Vicmarie Marrero-Colon**[1], **Sanya Mehta**[1], **Dereje D. Jima**[1,2], **Seh Hoon Oh**[3], **Anna Mae Diehl**[3], **Tiffany Fougeray**[4], **Hervé Guillou**[4], **Michael Cowley**[1]

[1]Department of Biological Sciences, Center for Human Health and the Environment, North Carolina State University, Raleigh, North Carolina, USA

[2]Bioinformatics Research Center, North Carolina State University, Raleigh, North Carolina, USA

[3]Department of Medicine, Duke University, Durham, North Carolina, USA

[4]UMR 1331, Institut National de la Recherche Agronomique, Toxalim (Research Center in Food Toxicology), Toulouse, France

Abstract

Background and Aims: Within the next decade, NAFLD is predicted to become the most prevalent cause of childhood liver failure in developed countries. Predisposition to juvenile NAFLD can be programmed during early life in response to maternal metabolic syndrome (MetS), but the underlying mechanisms are poorly understood. We hypothesized that imprinted genes, defined by expression from a single parental allele, play a key role in maternal MetS-induced NAFLD, due to their susceptibility to environmental stressors and their functions in liver homeostasis. We aimed to test this hypothesis and determine the critical periods of susceptibility to maternal MetS.

Approach and Results: We established a mouse model to compare the effects of MetS during prenatal and postnatal development on NAFLD. Postnatal but not prenatal MetS exposure is associated with histological, biochemical, and molecular signatures of hepatic steatosis and

Correspondence: Michael Cowley, Ph.D., Department of Biological Sciences, Center for Human Health and the Environment, North Carolina State University, Campus Box 7633, Raleigh, NC 27695, USA. macowley@ncsu.edu.

AUTHOR CONTRIBUTIONS

Marine Baptissart, Michael Cowley: conception and design, acquisition of data, analysis and interpretation of data, drafting of the article and revising it critically, final approval of the version to be published. Christine M. Bradish, Brie S. Jones, Evan Walsh, Jesse Tehrani, Vicmarie Marrero-Colon, Sanya Mehta, Seh Hoon Oh, Tiffany Fougeray: acquisition of data. Dereje D. Jima: analysis of data. Anna Mae Diehl, Hervé Guillou: interpretation of data.

CONFLICTS OF INTEREST

Nothing to report.

SUPPORTING INFORMATION

Additional supporting information may be found in the online version of the article at the publisher's website.

ETHICS STATEMENT

Animal work was approved by the North Carolina State University Institutional Animal Care and Use Committee (protocols 15–013-B and 19–049-B).

fibrosis in juvenile mice. Using RNA sequencing, we show that the Imprinted Gene Network (IGN), including its regulator *Zac1*, is up-regulated and overrepresented among differentially expressed genes, consistent with a role in maternal MetS-induced NAFLD. In support of this, activation of the IGN in cultured hepatoma cells by overexpressing *Zac1* is sufficient to induce signatures of profibrogenic transformation. Using chromatin immunoprecipitation, we demonstrate that Zac1 binds the *TGF-β1* and *COL6A2* promoters, forming a direct pathway between imprinted genes and well-characterized pathophysiological mechanisms of NAFLD. Finally, we show that hepatocyte-specific overexpression of *Zac1* is sufficient to drive fibrosis in vivo.

Conclusions: Our findings identify a pathway linking maternal MetS exposure during postnatal development to the programming of juvenile NAFLD, and provide support for the hypothesis that imprinted genes play a central role in metabolic disease programming.

INTRODUCTION

NAFLD describes a spectrum of chronic liver defects ranging from steatosis, characterized by excess accumulation of lipids in hepatocytes, to NASH at more advanced stages. The histological features of NASH include inflammation, hepatocyte ballooning, cell death, and fibrosis leaving the patient at increased risk for liver failure and/or HCC.

With a prevalence of 30% in the United States, NAFLD is a major public health concern.[1] While changes to nutrition, socioeconomic status, and lifestyle constitute major risk, predisposition to NAFLD may be predetermined during perinatal life in response to environmental stressors, a process called developmental programming. In support of an early life origin, recent data show that NAFLD is being diagnosed at increasingly younger ages, with 10% of the pediatric population affected.[2,3]

Non-human primate and rodent studies have shown that a key developmental stressor that primes the infant liver for increased NAFLD susceptibility is maternal metabolic syndrome (MetS).[4] Despite a robust link having been established between maternal MetS and offspring NAFLD, two key questions remain unanswered: (1) Is exposure to maternal MetS during prenatal or postnatal development more significant in the early onset of NAFLD? and (2) What is the nature of the primary causative molecular events? Addressing these knowledge gaps would allow for improved disease prediction and potentially enable therapeutic intervention prior to NAFLD onset.

Although it is unclear how maternal MetS programs NAFLD, the molecular mechanisms driving the pathogenesis of the disease are well described.[5] These include reprogramming of transcriptional networks involved in lipid metabolism, inflammation, and reactive oxygen species production. The cytokine TGF-β1 controls signaling pathways and transcriptional programs central for the progression of NAFLD to advanced stages characterized by fibrosis. TGF-β1 mediates TGF-βR1 activation and phosphorylation of the receptor-associated mothers against decapentaplegic homologs (SMADs) (R-SMADs) 2 and 3. Activated R-SMADs form a trimeric complex with SMAD4, which translocates to the nucleus and regulates target gene expression. TGF-β1 induces epithelial-to-mesenchymal transition (EMT) in hepatocytes[6] and activates HSCs to myofibroblasts,[7] both effects contributing to collagen production, extracellular matrix deposition, and fibrosis.

In animal models of maternal MetS-induced NAFLD, misregulation of these metabolic pathways has been reported.[5] However, because most studies rely on targeted approaches often limited to the advanced timing of adulthood when the disease pathology is already established, the primary molecular events linking maternal MetS exposure to the reprogramming of down-stream metabolic networks are poorly understood. Epigenetic changes have been proposed as primary causative events in NAFLD programming,[8,9] but it is unclear how these changes modulate gene transcription networks, leading to a disease state.

Imprinted genes, defined by their expression from a single parental allele (maternal or paternal), are subject to multiple layers of epigenetic regulation.[10] These include allele-specific patterns of DNA methylation and posttranslational histone modifications established at imprinting control regions (ICRs). Work from our lab and others has shown that DNA methylation at ICRs is uniquely sensitive to disruption by maternal conditions during early life.[11,12] Moreover, once established, ICR epigenetic states are maintained throughout life; thus, environmentally induced changes in development could have long-term effects on imprinted gene expression. Imprinted genes play critical roles in regulating metabolism; phenotypes resulting from imprinted gene manipulation are often associated with liver disease.

Based on this unique set of properties, we hypothesize that imprinted gene dysregulation is an important mechanism in the developmental programming of NAFLD in response to maternal MetS. Using a mouse model of MetS-induced NAFLD, we show that postnatal, but not prenatal, exposure to maternal MetS is associated with steatosis and fibrosis in the liver of juvenile mice. This is associated with activation of the Imprinted Gene Network (IGN), including its master transcription factor Zac1 (also called Plagl1), consistent with the idea that imprinted genes play a role in MetS-induced NAFLD. In further support of our hypothesis, we demonstrate that artificial activation of *Zac1* and the IGN in cultured hepatocytes stimulates TGF-β1 signaling, leading to extracellular matrix deposition, key events in the pathophysiology of NAFLD. Furthermore, we demonstrate that hepatocyte-specific overexpression of *Zac1* in vivo is sufficient to induce molecular and histological signatures of fibrosis.

Together our data identify Zac1 and the IGN as a pathway linking maternal MetS exposure during postnatal development to the activation of well-characterized mechanisms driving NAFLD in the juvenile liver. Our data identify potential molecular markers that are predictive of NAFLD susceptibility.

EXPERIMENTAL PROCEDURES

Animal models

C57Bl/6J female F0 mice were fed a 10% or 45% fat diet (“control” [Ct] and “high fat” [HF] diet, respectively) from 3 weeks of age for 7 weeks (7w) or 17 weeks (17w), and mated to males fed a control diet. A glucose tolerance test (GTT) was performed 2 weeks before mating as described.[13] On the day of birth, F1 litters were standardized to five pups and

cross-fostered to dams who had given birth on the same day. A GTT was performed on F1 mice in the 7w cohort at postnatal day (PND) 16.

To overexpress *Zac1* in hepatocytes in vivo, 9-week-old mice were injected with adeno-associated virus 8 (AAV8)-TBG-*Zac1* or AAV8-TBG–enhanced green fluorescent protein (*EGFP*) particles through the tail vein.

The numbers of animals and litters represented in each analysis are presented in Table S1.

Histological and lipid analyses

Liver lobes were fixed in 4% formaldehyde and paraffin embedded for hematoxylin and eosin (H&E), sirius red staining and immunostaining, or flash frozen and cryo-sectioned for Oil Red O staining. Lipid content was determined by gas-liquid chromatography as described.[14]

In vitro models

Alpha mouse liver 12 (AML12), HepG2, and HEK293T cells were obtained from ATCC and cultured according to ATCC guidelines. LX-2 cells were a gift from Prof. Scott Friedman (Icahn School of Medicine at Mount Sinai). For transient transfection, AML12 cells were transfected with pLenti-CMV-Zac1-FLAG or pLenti-CMV-EGFP using Lipofectamine 2000. For stable transduction, lentivirus was produced using HEK293T cells as described.[15] HepG2 and LX-2 cells were transduced with virus carrying pLenti-CMV-Zac1-FLAG or pLenti-CMV-EGFP.

RNA analyses

RNA was isolated from cells and liver samples using the NucleoSpin kit (Macherey Nagel). cDNA was synthesized using Moloney-murine leukemia virus reverse transcriptase (Promega) and diluted for quantitative PCR. Primers are given in Table S2. RNA-sequencing (RNA-seq) libraries were constructed using NEBNext Ultra Directional RNA Library Prep Kit and NEBNext Mulitplex Oligos for Illumina (NEB). Quality control filtering, read mapping, and analysis of differential expression were performed as described.[16]

DNA methylation analysis

DNA was isolated from liver samples using phenol/chloroform and bisulfite-treated with the EZ DNA Methylation-Gold kit (Zymo). A subregion of the *Zac1* ICR was amplified by PCR, and methylation was quantified by pyrosequencing (PyroMark Q24, Qiagen). Primers are given in Table S2.

Protein analyses and chromatin immunoprecipitation

Protein extraction for western blotting was performed using radio immunoprecipitation assay buffer (Thermo Fisher Scientific) with protease inhibitors (Sigma Aldrich). Chromatin immunoprecipitation was performed as described previously.[17] Binding enrichment was determined by quantitative PCR using primers found in Table S2.

ELISAs

TGF-β1 and COL1A1 were measured in cell culture supernatants using DuoSet ELISA kits (R&D Systems).

Statistical analyses

Statistical analyses were performed using GraphPad software. Data were analyzed using one-way ANOVA followed by Dunnett's multiple comparison test, un-paired *t* tests or nested *t* tests, as indicated in the results.

Full Materials and Methods are presented in the Supporting Information.

RESULTS

Exposure to maternal MetS during postnatal development primes early onset of NAFLD and is associated with neonatal obesity and diabetes

MetS was induced in F0 female mice through consumption of a HF diet for 7 or 17 weeks (7w and 17w cohorts, respectively). Compared with sibling mice consuming a Ct diet, HF diet-fed mice showed increased body mass (Figure S1A) and significant intolerance to glucose (Figure S1B,C), two phenotypic traits characteristic of MetS. While the increase in body mass was significantly higher in 17w than 7w mice, the HF diet duration had no significant impact on glucose intolerance (Figure S1A,C).

Ct and MetS females from both the 7w and 17w cohorts were mated to control males generating the experimental F1 offspring. F1 mice exposed to maternal MetS *in utero* presented with increased body mass at birth (PND0) when compared with controls (Figure 1A). F1 pups from 17w MetS dams were significantly heavier than pups from 7w MetS dams. Maternal MetS did not influence pregnancy rate, litter size, sex ratio, or F1 mortality at birth (Table S3).

To enable distinction between the effects of maternal MetS exposure during prenatal and postnatal development, F1 pups were cross-fostered between control and MetS dams on the day of birth, generating four experimental groups within each of the 7w and 17w cohorts (Figure 1B). Fed glycemia levels and glucose tolerance were measured at PND16 in pups from the 7w cohort only. F1 mice exposed to maternal MetS during postnatal (Ct-MetS and MetS-MetS), but not prenatal life (MetS-Ct), showed an increase in fed glycemia levels compared with control mice (Ct-Ct) (Figure 1C) as well as an impairment in their response to a GTT (Figure 1D). At PND21, Ct-MetS mice from both the 7w and 17w cohorts presented with increased body mass, primarily due to excessive accumulation of retroperitoneal white adipose tissue (Figure 1E,F). HF diet duration had no detectable effects on these outcomes.

Importantly, these phenotypes were associated with the onset of NAFLD at PND21. Ct-MetS and MetS-MetS mice presented with increased liver weight in the 17w but not the 7w cohort (Figure 2A). Histopathological analysis identified excess neutral lipid storage in Ct-MetS and MetS-MetS hepatocytes in both the 7w and 17w cohorts (Figure 2B,C). This was confirmed by biochemical analysis of triacylglycerides in the 7w cohort (Figure 2D).

Given that F1 mice from the 7w and 17w cohorts presented with similar histopathologies, our subsequent analyses focused on the 7w mice only. Sirius red staining revealed the presence of fibrotic tissue in the livers of Ct-MetS and MetS-MetS, but not Ct-Ct and MetS-Ct mice (Figure 2B), indicative of an advanced stage of NAFLD induced by postnatal exposure to maternal MetS. Most of the fibrosis was observed around the central vein with extensions into the midzone (Figure S2). When quantified, these differences were not statistically significant (Ct-Ct vs. Ct-MetS: q value = 0.28; Ct-Ct vs. MetS-MetS: q value = 0.31)—most likely due to high variability among individuals of the same group (Bartlett's p value = 0.01) (Figure 2E). Immunohistochemical staining for F4/80$^+$ cells, representing liver-resident Kupffer cells and infiltrating macrophages, in Ct-Ct and Ct-MetS livers did not reveal differences in the number or distribution of these cells (Figure S3).

Taken together, our results show that exposure to maternal MetS during postnatal, but not prenatal, development programs obesity, diabetes, and NAFLD at juvenile ages.

Exposure to maternal MetS during postnatal development recapitulates the transcriptomic signature of advanced NAFLD

To understand the molecular basis for differences in the hepatic response to prenatal and postnatal maternal MetS exposure, RNA-seq was performed on F1 livers from the 7w cohort at PND21.

Only 12 DEGs (q value ≤ 0.05) were identified between Ct-Ct and MetS-Ct animals, consistent with no detectable impact of prenatal exposure to maternal MetS at the histological level. In contrast, 408 and 1275 genes were differentially expressed in Ct-MetS and MetS-MetS livers, respectively, when compared with controls (Figure 3A; Table S4).

These results demonstrate that exposure to maternal MetS during postnatal development alone is sufficient to trigger widespread transcriptomic changes in the liver. Therefore, DEGs between Ct-Ct and Ct-MetS livers were chosen for further functional analysis. Using Ingenuity Pathway Analysis (IPA), the 25 "diseases or functions" most enriched among DEGs included terms related to glucose and lipid metabolism, inflammation, oxidative stress and fibrosis, thereby recapitulating the molecular signature of the entire NAFLD spectrum (Figure 3B; Table S5). Additional terms that were significantly enriched referred to liver failure or HCC. Additionally, the top 12 predicted "upstream regulators" were all implicated in NAFLD pathogenesis. Of these, the cytokine TGF-β1 showed the highest positive z score (p value = 4.01E-12; z score = 3.695), suggesting that this key pro-fibrotic pathway is activated in Ct-MetS livers.

Postnatal exposure to maternal MetS is associated with activation of *Zac1* and the IGN

Our central hypothesis proposes that imprinted gene dysregulation plays a key role in NAFLD programming in response to maternal MetS. In support of this, transcripts of the paternally expressed imprinted gene *Zac1* were significantly increased in PND21 Ct-MetS livers compared with controls, but not in MetS-Ct or MetS-MetS livers (Figure 4A). This is consistent in F1 mice from the 7w and 17w cohorts, without a significant effect of HF diet duration.

We hypothesized that the increased expression of *Zac1* in Ct-MetS mice is caused by perturbation of DNA methylation at the *Zac1* ICR. Ct-Ct mice showed the expected approximate 50% methylation, reflecting one methylated and one unmethylated allele, but this was not significantly altered in Ct-MetS mice, suggesting that the increase in *Zac1* expression is independent of DNA methylation state (Figure 4B).

Zac1 encodes a nuclear transcription factor, which is a master regulator of a coordinately expressed transcriptional network termed the IGN.[18] The IGN consists of 325 biallelically expressed genes and 84 imprinted genes including *Zac1* itself.[19] The IGN is implicated in several physiological processes including muscle regeneration and adipocyte differentiation. Despite evidence for the conservation of the IGN in hepatic tissue,[18] its functional relevance for liver physiology has not previously been demonstrated.

To address this, we first took an unbiased approach to identify functions that are enriched among the 409 IGN genes. Functional analysis using IPA showed that IGN genes are highly predictive of “hepatic fibrosis” (p value = 3.89E-10) with the pro-fibrogenic cytokine TGF-β1 being identified as the top predicted upstream regulator (p value = 2.89E-37) (Table S6).

Given this finding showing the potential relevance of the IGN to NAFLD, we next sought to determine whether the up-regulation of *Zac1* in Ct-MetS livers was associated with changes to IGN transcript accumulation. In our RNA-seq data, IGN members were significantly overrepresented among DEGs between Ct-MetS and Ct-Ct mice (enrichment ×2.92; p value = 0.00012; hypergeometric test) (Figure 4C; Table S7). Of note, significantly more IGN genes were increased in expression (25 genes) than decreased in expression (four genes) (chi-squared test; $p \leq 0.0001$; expected values to be equal) (Figure 4D). Interestingly, 17 of the 29 differentially expressed IGN genes have previously been associated with NAFLD (Figure 4E; Table S7). Among these, seven underlie the predicted activation of the Tgf-β1 pro-fibrotic pathway generated by IPA analysis (Tables S6 and S7).

A subset of IGN members showing differential expression by RNA-seq and with relevance to NAFLD and/or Tgf-β1 signaling were selected for validation by quantitative reverse-transcription PCR on livers from both 7w and 17w mice. Consistent with RNA-seq, most of these transcripts showed a significant increase in expression in Ct-MetS mice compared with controls (Figure 4F). With the exception of *Gpx7* in the 17w cohort, the transcriptional response of these IGN genes was significantly correlated with *Zac1* expression (p value ≤ 0.05; Spearman rank order correlation test).

Four additional IGN genes implicated in fibrosis (*Col1a1*, *Col6a2*, *Col14a1*, and *Mmp2*) that were not identified as being differentially expressed by RNA-seq showed increases in expression in Ct-MetS livers when assayed by quantitative real-time PCR. For each of these, expression was significantly correlated with *Zac1* expression (Figure 4F).

Given that the functional analysis of our transcriptomic data provided strong evidence for the activation of Tgf-β1 signaling, we assayed *Tgf-β1* transcript abundance by quantitative PCR and detected a significant increase in Ct-MetS livers compared with controls in mice from the 7w and 17w cohorts (Figure 4G).

The IGN is conserved in cultured hepatocytes following *Zac1* overexpression.

The IGN has been described in several cell types and tissues in mouse (embryonic fibroblasts, 3T3-L1 preadipocytes, Neuro2a neuroblastoma cells, whole liver) and human (placenta).[18–21] Hepatocytes represent 80% of the cell population of the liver. To determine whether the IGN is conserved specifically in this major liver cell type, cultured mouse hepatocytes (AML12 cells) were transfected with overexpression constructs containing either the *Zac1* or *EGFP* open reading frames, and the resulting global transcriptional changes were analyzed by RNA-seq.

Overexpression of *Zac1* led to differential expression of 733 genes when compared with the transcriptome of cells overexpressing *EGFP* (q value ≤ 0.05) (Figure 5A; Table S8). Among these DEGs, members of the IGN were significantly overrepresented (enrichment ×1.67; p value = 0.0094; hypergeometric test) (Figure 5A; Table S9). As observed in Ct-MetS mice, significantly more IGN genes were increased in expression (17 genes) than decreased in expression (seven genes) upon *Zac1* overexpression ($p \leq 0.0412$; chi-squared test; expected values to be equal) (Figure 5B).

Zac1 overexpression and IGN activation in cultured hepatoma cells is sufficient to promote TGF-β1 signaling, resulting in fibrotic trans-differentiation and extracellular matrix deposition

We next sought to determine whether *Zac1* overexpression and IGN activation within hepatocytes is sufficient to mimic the molecular signature and functional outcomes underlying NAFLD programming observed in Ct-MetS mice.

Functional analysis of RNA-seq from AML12 cells revealed Tgf-β1 as one of the top upstream regulators underlying differential gene expression (p value = 1.43E-09; Table S10). This result, consistent with the transcriptional signature observed in vivo, suggests that *Zac1* and the IGN may be sufficient to induce pro-fibrogenic transformation of hepatocytes. To test this hypothesis, we developed a model of long-term *Zac1* overexpression in the human hepatoma cell line HepG2.

HepG2 cells overexpressing *Zac1* showed a significant increase in *TGF-β1* transcripts compared with *EGFP*-expressing controls (Figure 6A). Additionally, these cells accumulated more TGF-β1 in their media (Figure 6B). Furthermore, the TGF-β1 signaling pathway was activated following *Zac1* overexpression, as demonstrated by increased levels of phospho-SMAD2/3 (Figure 6C).

TGF-β1-mediated profibrogenic transformation involves activation of the transcription factor snail family transcriptional repressor 1 (SNAI1), which represses the epithelial marker E-cadherin, encoded by the *CADH1* gene. Consistent with TGF-β1 pathway activation, HepG2 cells overexpressing *Zac1* showed increased expression of *SNAI1* (Figure 6D) with an associated decrease in *CADH1* transcript and E-cadherin protein (Figure 6E,F). These changes were associated with increased accumulation of *COL6A2* and *COL1A1* transcripts, encoding major components of extracellular matrix (ECM) (Figure 6G,H). Moreover, we observed increased collagen deposition in *Zac1* overexpressing cells, as measured by an ELISA of pro-COL1A1, suggestive of an accumulation of ECM underlying fibrotic events

(Figure 6I). Overexpression of *Zac1* in the HSC line LX-2 had no effect on *COL1A1* expression and only negligible impact on *COL6A2*, suggesting that this mechanism may be specific to hepatocytes (Figure S4).

Zac1 overexpression also caused significantly increased expression of *Tgf-β1*, *Snai1*, *Col6a2*, and *Col1a1* in AML12 cells, despite the transient nature of the *Zac1* overexpression system, indicative of conservation of this mechanism between mouse and human hepatocytes (Figure S5).

Zac1 binds the promoters of pro-fibrogenic genes

Given the strong association between *Zac1* overexpression and the expression of pro-fibrogenic genes in hepatocytes, we next sought to determine whether Zac1 directly controls transcription of the *TGF-β1*, *SNAI1*, *COL6A2*, and *COL1A1* genes by binding to their promoters.

Computational analyses identified at least one Zac1 consensus binding site within 1 kb of each of the annotated transcriptional start sites (TSSs) of these genes (Figure 7A,B; Figure S6). Zac1 binding was assayed by chromatin immunoprecipitation followed by quantitative PCR on HepG2 cells overexpressing *Zac1*. None of the predicted binding sites at the *SNAI1* and *COL1A1* promoter regions showed enrichment for Zac1 binding (Figure S6). However, compared with control cells overexpressing *EGFP*, Zac1 binding was significantly enriched at one predicted binding site at each of the *TGF-β1* and *COL6A2* promoter regions (Figure 7A,B). This suggests that Zac1 is involved in the direct transcriptional regulation of these key drivers of NAFLD progression.

Artificial overexpression of *Zac1* in hepatocytes in vivo induces molecular and histological signatures of fibrosis

Finally, we asked whether overexpression of *Zac1* in hepatocytes is sufficient to induce fibrosis in vivo. Mice were injected with AAV8 particles carrying overexpression constructs containing *Zac1* or *EGFP* driven by the TBG promoter. Hepatocyte-specific expression was confirmed by immunofluorescence (Figure S7A). At 3 weeks following injection, AAV8-TBG-*Zac1* livers showed increased expression of *Zac1* and a subset of IGN genes that are markers of fibrosis (Figure 8A; Figure S7B). At 10 weeks following injection, *Zac1* overexpression was associated with histological hallmarks of fibrosis in the subcapsular region, including disorganization of the sinusoid, apoptotic hepatocytes, and increased sirius red staining compared with controls (Figure 8B). Additionally, immunofluorescence experiments demonstrated an increase in α-smooth muscle actin, a marker of activated stellate cells, at 10 weeks following injection in AAV8-TBG-*Zac1* livers (Figure S7A). Together, these data strongly suggest that *Zac1* overexpression in hepatocytes is sufficient to drive fibrosis in vivo in the absence of maternal MetS.

DISCUSSION

NAFLD has emerged as one of the most common chronic liver diseases in the pediatric population. Epidemiological studies demonstrate that women with MetS predispose their infant toward developing NAFLD, an issue of major concern given that approximately half

of women beginning pregnancies in the United States are overweight or obese.[22] Despite this link being well-established, the underlying mechanisms remain largely unknown.

Here, we demonstrate in mice that exposure to maternal MetS during postnatal, but not prenatal, development is associated with the early onset of NAFLD. Transcriptomic analyses identify the IGN, including its master transcription factor Zac1, as being up-regulated in the liver of susceptible mice. By overexpressing *Zac1* in cultured hepatoma cells, we show that activation of the IGN stimulates fibrotic pathways and ECM deposition—key events driving NAFLD progression. Importantly, overexpression of *Zac1* in hepatocytes in vivo is sufficient to activate a subset of fibrosis-associated IGN genes and induce mild fibrosis.

Our results identify the IGN as an important contributor to the progression of juvenile NAFLD in response to maternal MetS exposure specifically during postnatal development.

Previous studies in rodents have focused primarily on the programming effects of maternal MetS on chronic liver disease at adulthood.[23,24] However, in addition to an increasing prevalence among adults, NAFLD affects 10% of the pediatric population in the United States.[3] Our mouse model supports a link between maternal MetS and juvenile NAFLD. We show that offspring exposed to maternal MetS during postnatal development present with steatosis as early as PND21, and that a subset of these individuals present with fibrosis, independent of histological evidence of inflammation. These results are highly reminiscent of the juvenile NAFLD dynamic observed in humans, because at the time of NAFLD diagnosis, 25%–50% of children have NASH and 10%–25% have advanced fibrosis.[25]

NAFLD is associated with systemic metabolic changes including insulin resistance and increased waist circumference, which are risk factors for type 2 diabetes and obesity.[26,27] In further support of the relevance of our model to human health, Ct-MetS mice showed impaired glucose tolerance and increased body weight. Although these systemic changes can promote NAFLD, our data from cultured hepatoma cells show that Zac1-induced activation of the IGN is sufficient to induce signatures of fibrogenic activity, supporting the hypothesis of a cell autonomous mechanism that is independent of systemic conditions.

Maternal MetS has been extensively modeled in rodents and primates through the use of hypercaloric diets.[28] The diversity of experimental designs, including differences in total energy count, fat content and lipid origin in the diet, as well as variation in the duration of exposure and animal age, has led to a wide range of maternal phenotypes from chronic to severe obesity with or without associated diabetes. This limits our understanding of the critical maternal phenotypic component driving the impact on offspring. In this study, we analyzed two cohorts, 7w and 17w, in which F0 female mice were exposed to different durations of HF diet feeding, leading to body weight gains of 4.2% and 11.3%, respectively, with similar glucose intolerance phenotypes. Except for F1 liver weight, we did not observe any differences in NAFLD susceptibility associated with the duration of maternal HF diet feeding. This indicates that even a subtle increase in maternal weight is sufficient to program early onset of NAFLD in offspring, and that this is independent of maternal glucose intolerance.

Most developmental programming studies of MetS have focused on the importance of *in utero* development. However, in humans, as well as in many animal models of programming, offspring continue to be exposed to maternal MetS after birth, during which time key developmental processes occur. In rodents, hepatocytes proliferate and differentiate for up to 30 days after birth (5 years in humans).[29] The period of postnatal development therefore represents a window of potential sensitivity to extrinsic factors. In this study, we implemented a cross-fostering design in mice to cleanly distinguish between the effects of maternal MetS exposure during prenatal and postnatal development. A striking finding from our work is that postnatal exposure to maternal MetS is sufficient to program juvenile NAFLD, whereas individuals exposed only during prenatal life do not present with any metabolic defect at the systemic or hepatic levels. Exposure to maternal MetS during both prenatal and postnatal development did not exacerbate NAFLD phenotypes or protect mice from the impacts of postnatal exposure alone.

Our study aimed to identify early molecular mechanisms linking maternal MetS to juvenile NAFLD susceptibility. We hypothesized that imprinted genes play an important role in this process. We and others have demonstrated previously that imprinted genes are particularly sensitive to the developmental environment and that their dysregulation can cause liver disease. For example, the imprinted long noncoding RNA *H19* promotes hepatic steatosis[30] and obstructive cholestatic liver fibrosis,[31] and *Grb10* regulates hepatic lipid metabolism in a cell autonomous manner.[32,33] Imprinted genes are coordinately regulated with a set of biallelically expressed genes as a transcriptional network, the IGN, which controls fetal growth, adipocyte differentiation, and muscle regeneration.[19] Here, using gene-set enrichment analysis, we show that members of the IGN are enriched in functions related to hepatic fibrosis, and demonstrate that activation of the IGN in hepatoma cells through overexpressing *Zac1* activates the pro-fibrogenic cytokine TGF-β1. Together, our findings from in vivo and in vitro models provide strong support for our hypothesis, suggesting that imprinted genes are key players linking the developmental environment to the activation of well-characterized mechanisms driving NAFLD pathogenesis. Ongoing work in our lab will address the individual contributions of IGN members to this process. In hepatoma cells, we have already demonstrated that Zac1 binds directly to the promoters of *TGF-β1*, and, intriguingly, *COL6A2*. Conservation of this binding has previously been described in Neuro2a cells.[20] These results suggest that Zac1 may drive NAFLD progression partly through a TGF-β1-independent mechanism.

Although lineage tracing experiments have demonstrated that hepatocytes can undergo EMT and contribute substantially to the population of fibroblasts that promote fibrosis,[34] HSCs also contribute to fibrosis.[35] In vitro, *Zac1* overexpression in HSCs failed to substantially activate collagen gene expression, and in vivo hepatocyte-specific *Zac1* overexpression was sufficient to induce molecular and histological signatures of fibrosis, including HSC activation. Together, these data suggest that *Zac1* functions primarily in hepatocytes in response to maternal MetS. Our ongoing work will test the hypothesis that hepatocytes overexpressing *Zac1* activate neighboring HSCs through secretion of TGF-β1, contributing to the fibrosis observed in Ct-MetS mice. Previous studies of *Zac1* overexpression in murine Neuro2a and insulinoma cells identified transcriptional changes in genes involved in ECM function and signaling, suggesting a role for *Zac1* in fibrogenesis in other tissues too.[20]

How maternal MetS activates *Zac1* in the postnatal liver is unknown. While we and others have shown that DNA methylation at ICRs is susceptible to perturbation by the environment, including maternal diet, this occurs during early prenatal development, after which the epigenetic state is fixed. This is consistent with our observation that postnatal exposure to maternal MetS does not alter DNA methylation at the *Zac1* ICR, and suggests that an alternative regulatory mechanism is responsible. *Zac1*, like other imprinted genes, is highly expressed during embryonic development and down-regulated during postnatal development, a process controlled through chromatin remodeling at ICRs.[36–38] We propose that maternal MetS impairs this mechanism of repression, sustaining high levels of imprinted gene expression after birth. We will test this hypothesis empirically.

Upstream of epigenetic and gene-expression changes, there are multiple mechanisms through which the metabolic state of the dam could affect offspring during postnatal development. For example, maternal care behavior can be modulated by HF diet feeding.[39] However, in a previous study exploiting the same cross-fostering model described here, we demonstrated that maternal diet had no direct effect on care behavior, and that maternal care was predominantly driven by the *in utero* environment experienced by the F1 offspring.[40] Given that Ct-MetS mice presenting with NAFLD were born to Ct dams and therefore did not experience an adverse *in utero* environment, we do not expect maternal behavior to be a significant mechanism in the observed programming of NAFLD. Further studies will be required to determine the nature of the signal that activates *Zac1* expression in the F1 liver.

Supplementary Material

Refer to Web version on PubMed Central for supplementary material.

ACKNOWLEDGMENTS

The authors thank John Cullen for guidance on interpreting pathology, Reiner Schulz for guidance on statistical analyses, and members of the Cowley Lab for helpful discussion of the work.

Funding information

National Institutes of Health (K22ES027510, R01ES031596, P30ES025128, P30DK034987 and T32ES007046); Oak Ridge Associated Universities through a Ralph E. Powe Junior Faculty Enhancement Award; and next-generation sequencing was performed by the NCSU Genomics Sciences Laboratory (Raleigh, NC)

Abbreviations:

17w	17-week cohort
7w	7-week cohort
AAV	adeno-associated virus
ANOVA	analysis of variance
Ct	control
DEG	differentially expressed gene

ECM	extracellular matrix
EGFP	enhanced green fluorescent protein
EMT	epithelial-to-mesenchymal transition
GTT	glucose tolerance test
H&E	hematoxylin and eosin
HCC	hepatocellular carcinoma
HF	high fat
HSC	hepatic stellate cell
ICR	imprinting control region
IGN	Imprinted Gene Network
IPA	Ingenuity Pathway Analysis
MetS	metabolic syndrome
NAFLD	non-alcoholic fatty liver disease
NASH	non-alcoholic steatohepatitis
PND	postnatal day
RNA-seq	RNA sequencing
rWAT	retriperitoneal white adipose tissue
TAG	triacylglyceride
TSS	transcriptional start site

REFERENCES

1. Le MH, Devaki P, Ha NB, Jun DW, Te HS, Cheung RC, et al. Prevalence of non-alcoholic fatty liver disease and risk factors for advanced fibrosis and mortality in the United States. PLoS One. 2017;12:e0173499. [PubMed: 28346543]
2. Berardis S, Sokal E. Pediatric non-alcoholic fatty liver disease: an increasing public health issue. Eur J Pediatr. 2014;173:131–39. [PubMed: 24068459]
3. Schwimmer JB, Deutsch R, Kahen T, Lavine JE, Stanley C, Behling C. Prevalence of fatty liver in children and adolescents. Pediatrics. 2006;118:1388–93. [PubMed: 17015527]
4. Brumbaugh DE, Friedman JE. Developmental origins of nonalcoholic fatty liver disease. Pediatr Res. 2014;75:140–7. [PubMed: 24192698]
5. Friedman SL, Neuschwander-Tetri BA, Rinella M, Sanyal AJ. Mechanisms of NAFLD development and therapeutic strategies. Nat Med. 2018;24:908–22. [PubMed: 29967350]
6. Giannelli G, Koudelkova P, Dituri F, Mikulits W. Role of epithelial to mesenchymal transition in hepatocellular carcinoma. J Hepatol. 2016;65:798–808. [PubMed: 27212245]
7. Dewidar B, Meyer C, Dooley S, Meindl-Beinker AN. TGF-β in hepatic stellate cell activation and liver fibrogenesis—updated 2019. Cells. 2019;8:1419.

8. Gallego-Durán R, Romero-Gómez M. Epigenetic mechanisms in non-alcoholic fatty liver disease: an emerging field. World J Hepatol. 2015;7:2497–502. [PubMed: 26523202]
9. Sookoian S, Gianotti TF, Burgueño AL, Pirola CJ. Fetal metabolic programming and epigenetic modifications: a systems biology approach. Pediatr Res. 2013;73(Pt 2):531–42. [PubMed: 23314294]
10. Tucci V, Isles AR, Kelsey G, Ferguson-Smith AC, Tucci V, Bartolomei MS, et al. Genomic imprinting and physiological processes in mammals. Cell. 2019;176:952–65. [PubMed: 30794780]
11. Cowley M, Skaar DA, Jima DD, Maguire RL, Hudson KM, Park SS, et al. Effects of cadmium exposure on DNA methylation at imprinting control regions and genome-wide in mothers and newborn children. Environ Health Perspect. 2018;126:037003. [PubMed: 29529597]
12. Susiarjo M, Sasson I, Mesaros C, Bartolomei MS. Bisphenol A exposure disrupts genomic imprinting in the mouse. PLoS Genet. 2013;9:e1003401. [PubMed: 23593014]
13. Baptissart M, Sèdes L, Holota H, Thirouard L, Martinot E, de Haze A, et al. Multigenerational impacts of bile exposure are mediated by TGR5 signaling pathways. Sci Rep. 2018;8:16875. [PubMed: 30443025]
14. Régnier M, Polizzi A, Smati S, Lukowicz C, Fougerat A, Lippi Y, et al. Hepatocyte-specific deletion of Pparα promotes NAFLD in the context of obesity. Sci Rep. 2020;10:6489. [PubMed: 32300166]
15. Tiscornia G, Singer O, Verma IM. Production and purification of lentiviral vectors. Nat Protoc. 2006;1:241–5. [PubMed: 17406239]
16. Hudson KM, Belcher SM, Cowley M. Maternal cadmium exposure in the mouse leads to increased heart weight at birth and programs susceptibility to hypertension in adulthood. Sci Rep. 2019;9:13553. [PubMed: 31537853]
17. Johnson DS, Mortazavi A, Myers RM, Wold B. Genome-wide mapping of in vivo protein-DNA interactions. Science. 2007;316:1497–502. [PubMed: 17540862]
18. Varrault A, Gueydan C, Delalbre A, Bellmann A, Houssami S, Aknin C, et al. Zac1 regulates an imprinted gene network critically involved in the control of embryonic growth. Dev Cell. 2006;11:711–22. [PubMed: 17084362]
19. Al Adhami H, Evano B, Le Digarcher A, Gueydan C, Dubois E, Parrinello H, et al. A systems-level approach to parental genomic imprinting: the imprinted gene network includes extracellular matrix genes and regulates cell cycle exit and differentiation. Genome Res. 2015;25:353–67. [PubMed: 25614607]
20. Varrault A, Dantec C, Le Digarcher A, Chotard L, Bilanges B, Parrinello H, et al. Identification of Plagl1/Zac1 binding sites and target genes establishes its role in the regulation of extracellular matrix genes and the imprinted gene network. Nucleic Acids Res. 2017;45:10466–80. [PubMed: 28985358]
21. Iglesias-Platas I, Martin-Trujillo A, Petazzi P, Guillaumet-Adkins A, Esteller M, Monk D. Altered expression of the imprinted transcription factor PLAGL1 deregulates a network of genes in the human IUGR placenta. Hum Mol Genet. 2014;23:6275–85. [PubMed: 24993786]
22. Deputy NP, Dub B, Sharma AJ. Prevalence and trends in prepregnancy normal weight—48 states, New York City, and District of Columbia, 2011–2015. MMWR Morb Mortal Wkly Rep. 2018;66:1402–7. [PubMed: 29300720]
23. Oben JA, Mouralidarane A, Samuelsson A-M, Matthews PJ, Morgan ML, Mckee C, et al. Maternal obesity during pregnancy and lactation programs the development of offspring non-alcoholic fatty liver disease in mice. J Hepatol. 2010;52:913–20. [PubMed: 20413174]
24. Bruce KD, Cagampang FR, Argenton M, Zhang J, Ethirajan PL, Burdge GC, et al. Maternal high-fat feeding primes steatohepatitis in adult mice offspring, involving mitochondrial dysfunction and altered lipogenesis gene expression. Hepatology. 2009;50:1796–808. [PubMed: 19816994]
25. Goyal NP, Schwimmer JB. The progression and natural history of pediatric nonalcoholic fatty liver disease. Clin Liver Dis. 2016;20:325–38. [PubMed: 27063272]
26. Patton HM, Yates K, Unalp-Arida A, Behling CA, Huang T-K, Rosenthal P, et al. Association between metabolic syndrome and liver histology among children with nonalcoholic fatty liver disease. Am J Gastroenterol. 2010;105:2093–102. [PubMed: 20372110]

27. Schwimmer JB, Pardee PE, Lavine JE, Blumkin AK, Cook S. Cardiovascular risk factors and the metabolic syndrome in pediatric nonalcoholic fatty liver disease. Circulation. 2008;118:277–83. [PubMed: 18591439]

28. Williams L, Seki Y, Vuguin PM, Charron MJ. Animal models of in utero exposure to a high fat diet: a review. Biochim Biophys Acta - Mol Basis Dis. 2014;1842:507–19.

29. Walthall K, Cappon GD, Hurtt ME, Zoetis T. Postnatal development of the gastrointestinal system: a species comparison. Birth Defects Res Part B Dev Reprod Toxicol. 2005;74:132–56.

30. Liu C, Yang Z, Wu J, Zhang LI, Lee S, Shin D-J, et al. Long noncoding RNA H19 interacts with polypyrimidine tract-binding protein 1 to reprogram hepatic lipid homeostasis. Hepatology. 2018;67:1768–83. [PubMed: 29140550]

31. Song Y, Liu C, Liu X, Trottier J, Beaudoin M, Zhang LI, et al. H19 promotes cholestatic liver fibrosis by preventing ZEB1-mediated inhibition of epithelial cell adhesion molecule. Hepatology. 2017;66:1183–96. [PubMed: 28407375]

32. Madon-Simon M, Cowley M, Garfield AS, Moorwood K, Bauer SR, Ward A. Antagonistic roles in fetal development and adult physiology for the oppositely imprinted Grb10 and Dlk1 genes. BMC Biol. 2014;12:771. [PubMed: 25551289]

33. Luo L, Jiang W, Liu H, Bu J, Tang P, Du C, et al. De-silencing Grb10 contributes to acute ER stress-induced steatosis in mouse liver. J Mol Endocrinol. 2018;60:285–97. [PubMed: 29555819]

34. Zeisberg M, Yang C, Martino M, Duncan MB, Rieder F, Tanjore H, et al. Fibroblasts derive from hepatocytes in liver fibrosis via epithelial to mesenchymal transition. J Biol Chem. 2007;282:23337–47. [PubMed: 17562716]

35. Tsuchida T, Friedman SL. Mechanisms of hepatic stellate cell activation. Nat Rev Gastroenterol Hepatol. 2017;14:397–411. [PubMed: 28487545]

36. Lui JC, Finkielstain GP, Barnes KM, Baron J. An imprinted gene network that controls mammalian somatic growth is down-regulated during postnatal growth deceleration in multiple organs. Am J Physiol Integr Comp Physiol. 2008;295:R189–96.

37. Kernohan KD, Jiang Y, Tremblay DC, Bonvissuto AC, Eubanks JH, Mann MRW, et al. ATRX partners with cohesin and MeCP2 and contributes to developmental silencing of imprinted genes in the brain. Dev Cell. 2010;18:191–202. [PubMed: 20159591]

38. Voon H, Hughes J, Rode C, De La Rosa-Velázquez I, Jenuwein T, Feil R, et al. ATRX plays a key role in maintaining silencing at interstitial heterochromatic loci and imprinted genes. Cell Rep. 2015;11:405–18. [PubMed: 25865896]

39. Connor KL, Vickers MH, Beltrand J, Meaney MJ, Sloboda DM. Nature, nurture or nutrition? Impact of maternal nutrition on maternal care, offspring development and reproductive function. J Physiol. 2012;590:2167–80. [PubMed: 22411006]

40. Baptissart M, Lamb HE, To K, Bradish C, Tehrani J, Reif D, et al. Neonatal mice exposed to a high-fat diet *in utero* influence the behaviour of their nursing dam. Proc R Soc B Biol Sci. 1891;2018:20181237.

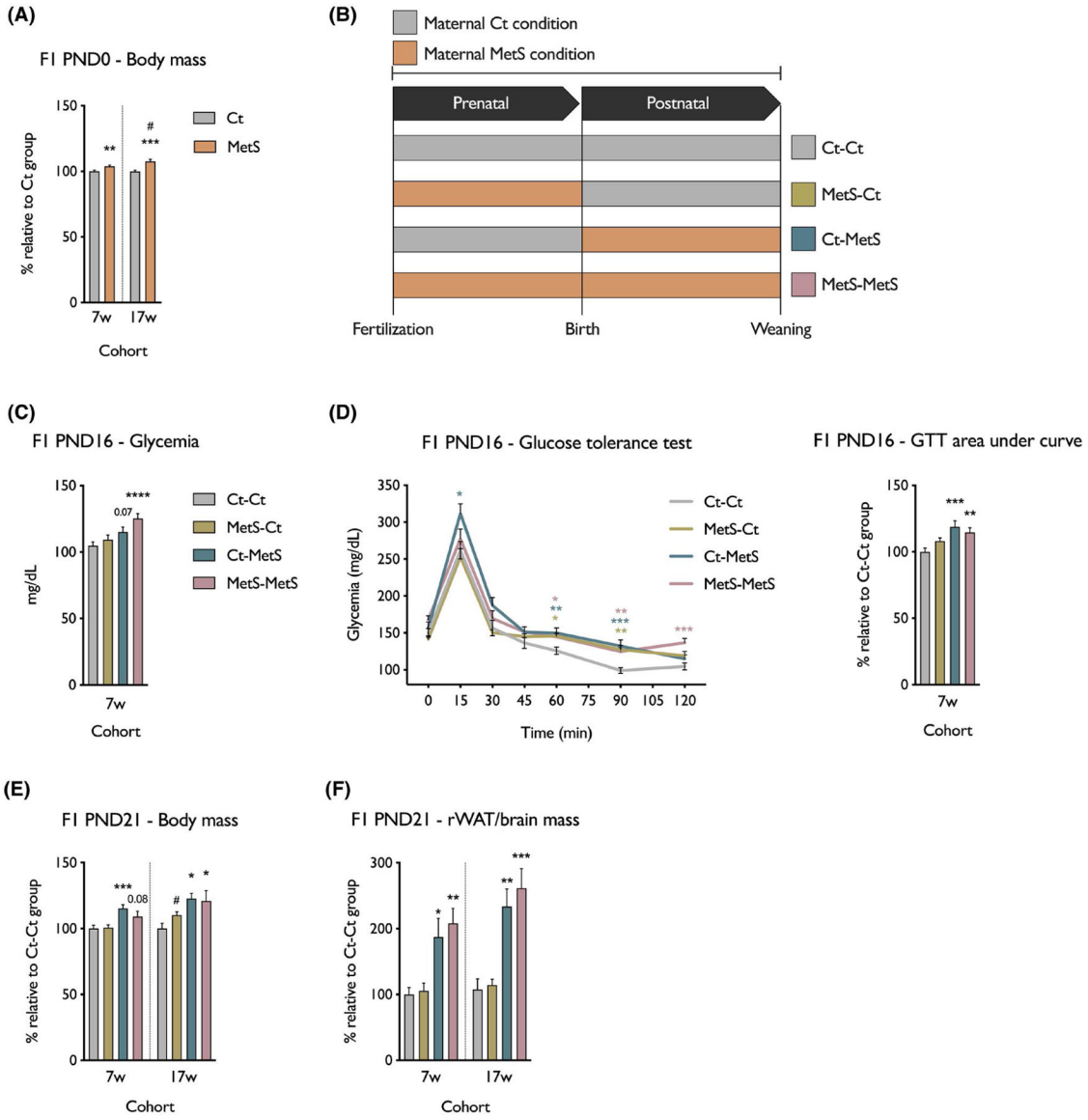

FIGURE 1.

F1 phenotypes in response to maternal metabolic syndrome (MetS) exposure. (A) Body mass at postnatal day (PND) 0. (B) Mice were cross-fostered at birth to generate four experimental groups. Groups are labeled in the format “prenatal-postnatal” exposure to maternal conditions control (Ct) or MetS. (C) Fed blood glycemia at PND16. (D) Glucose tolerance test (GTT) at PND16 (*left*) and corresponding AUC (*right*). (E) Body mass at PND21. (F) Retroperitoneal white adipose tissue (rWAT) mass relative to brain mass at PND21. Sexes are pooled. Data are presented as means ± SEM. *$p < 0.05$, **$p < 0.01$, ***$p < 0.001$. One-way ANOVA with Dunnett’s *post hoc* test comparing MetS-Ct, Ct-MetS, and MetS-MetS to Ct-Ct within the same cohort (*). Student’s *t* test, two-tailed, comparing 7-week (7w) to 17-week (17w) cohorts for the same exposure group (#)

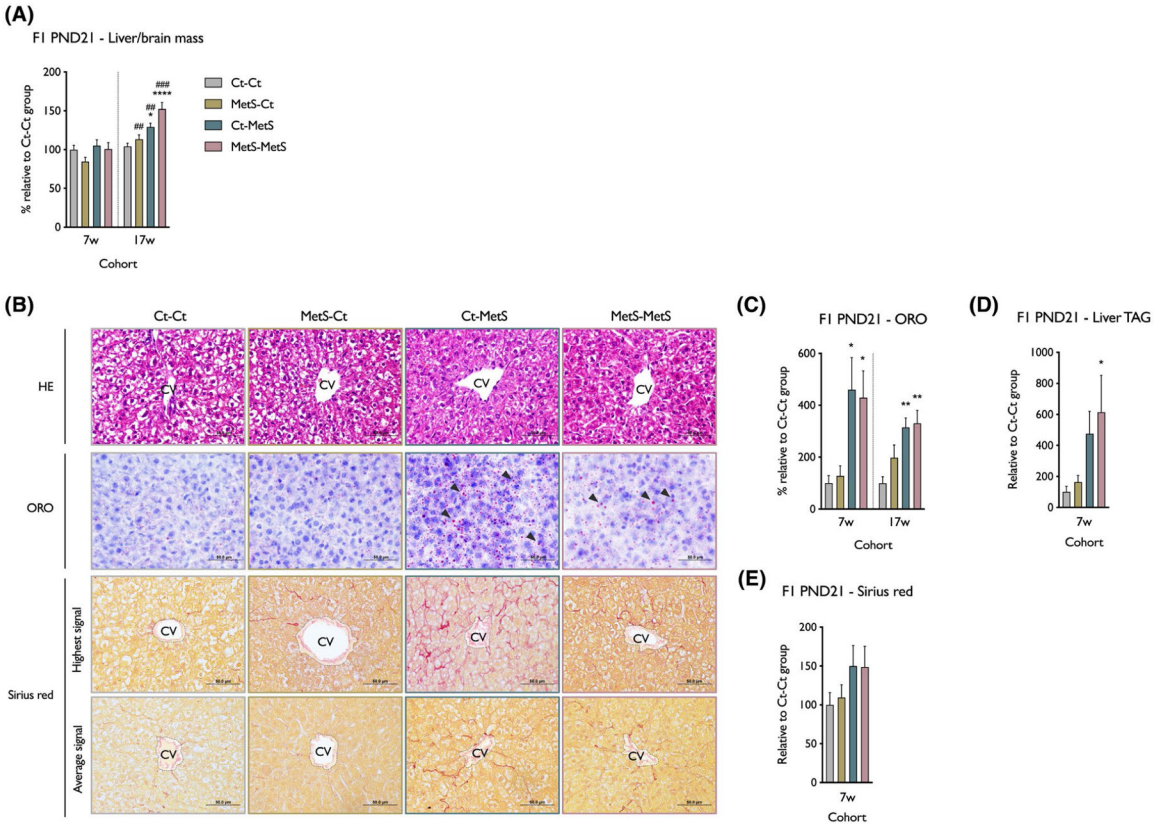

FIGURE 2.

Effect of maternal MetS on NAFLD programming at PND21. (A) Liver mass relative to brain mass at PND21. (B) Representative photomicrographs (magnification ×40) of liver sections. Top row: Hematoxylin and eosin (H&E) staining. Second row: Oil Red O (ORO) staining; arrowheads indicate neutral lipid droplets. Third and fourth rows: Sirius red staining, representing the highest and average signal within each group, respectively. (C) Digital quantification of ORO signal shown in (B). (D) Hepatic content of triacylglycerol (TAG). (E) Digital quantification of sirius red signal shown in (B). Sexes are pooled. Data are presented as means ± SEM. $*p < 0.05$, $**p < 0.01$, $***p < 0.001$. One-way ANOVA with Dunnett's *post hoc* test comparing MetS-Ct, Ct-MetS, and MetS-MetS to Ct-Ct within the same cohort (*). Student's *t* test, two-tailed, comparing 7w to 17w cohorts for the same exposure group ($^{\#}$). CV, central vein

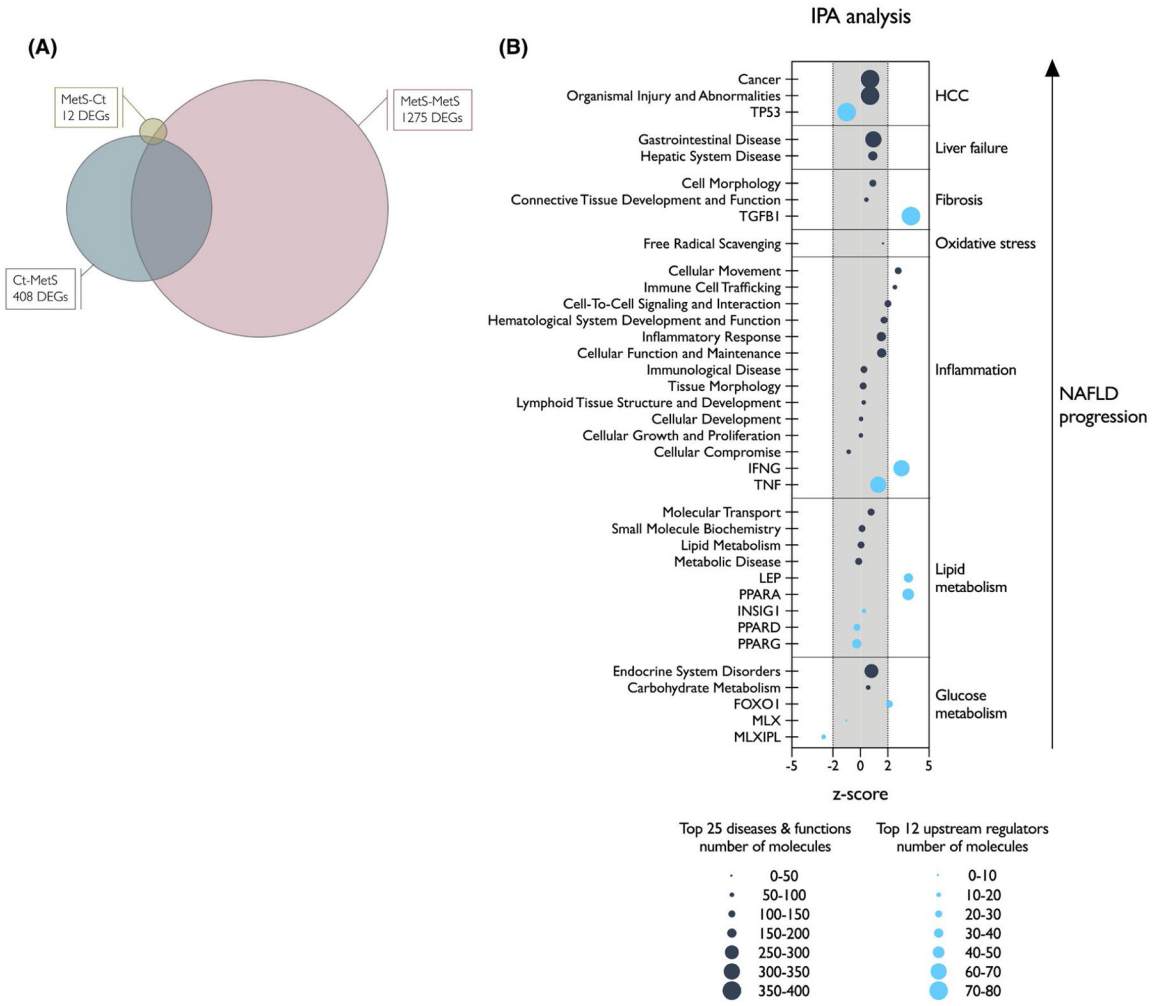

FIGURE 3.

RNA-sequencing (RNA-seq) analysis on F1 livers at PND21. (A) Venn diagram representing the number of differentially expressed genes (DEGs) for each exposure group and their intersection. DEGs are defined by $q < 0.05$ comparing MetS-Ct, Ct-MetS, and MetS-MetS to Ct-Ct females. (B) Graphical representation of Ingenuity Pathway Analysis (IPA) of the Ct-MetS DEGs. Circles indicate the top 25 diseases and functions (dark blue) and the top 12 upstream regulators (light blue). Circle size is proportional to the number of genes associated with the corresponding term. The x-axis displays the predicted direction of the effect as quantified by z scores ($z < 2$ = significant predicted negative effect; $z > 2$ = significant predicted positive effect). Diseases and functions and upstream regulators were grouped according to their functional relevance and sorted to match stages of NAFLD progression. PPAR, peroxisome proliferator-activated receptor

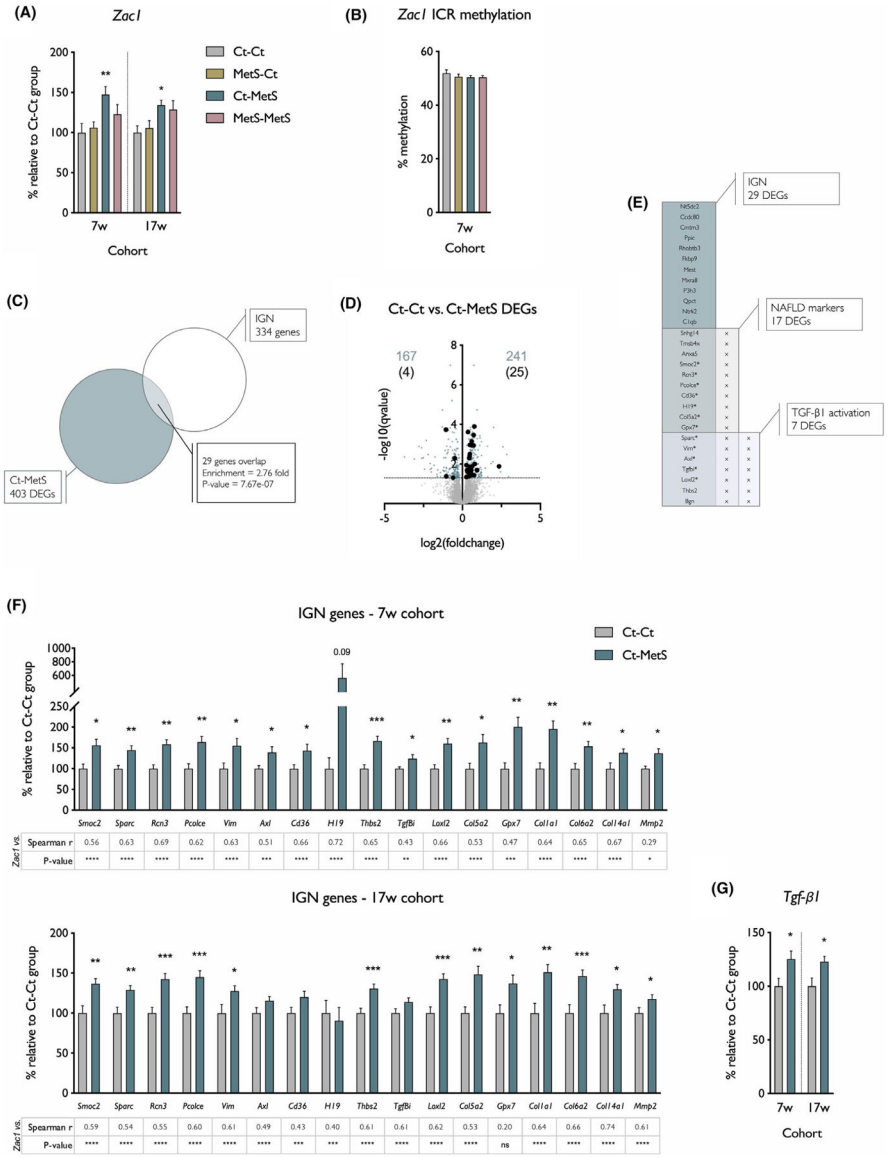

FIVGURE 4.

Imprinted Gene Network (IGN) expression in Ct-MetS livers. (A) *Zac1* transcript accumulation in F1 livers at PND21. Sexes are pooled. (B) Quantification of DNA methylation across six cytosine-guanine dinucleotides within the *Zac1* imprinting control region (ICR). (C) RNA-seq on livers from PND21 females. Venn diagram represents the number of Ct-MetS DEGs (defined by $q < 0.05$ comparing MetS-Ct to Ct-Ct) and their intersection with the IGN. Only IGN genes detected in RNA-seq are considered. Overrepresentation analysis was performed using a hypergeometric test. (D) Volcano plot of 13,038 genes identified through RNA-seq. The 408 DEGs in the Ct-MetS group are represented with blue dots. The DEGs identified as IGN members are indicated by bold black dots. (E) List of the 29 IGN genes identified as Ct-MetS DEGs (*left*). Check marks in overlapping boxes indicate those genes that have previously been identified as markers of NAFLD (*middle*) and TGF-β1 activation (*right*). (F) Selected RNA-seq hits validated

by quantitative reverse-transcription PCR on PND21 F1 livers from the 7w (*top*) and 17w (*bottom*) cohorts. Tables below each graph indicate the correlation between the expression of *Zac1* and each gene in F1 livers. Sexes are pooled. (G) *Tgf-β1* transcript accumulation in F1 livers at PND21. Sexes are pooled. Data are presented as means ± SEM. *$p < 0.05$, **$p < 0.01$, ***$p < 0.001$. Student's *t* test, two-tailed, comparing Ct-MetS to Ct-Ct within the same cohort

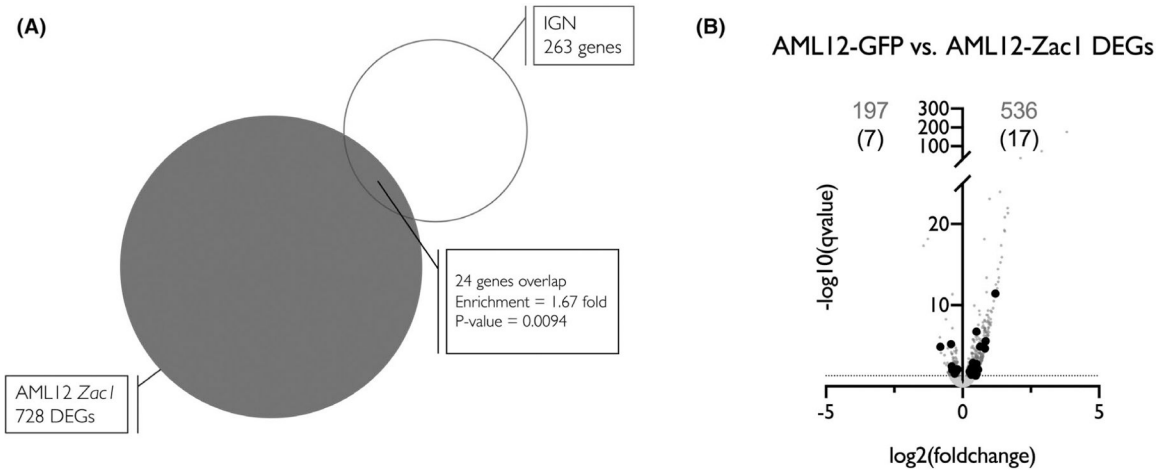

FIGURE 5.

RNA-seq analysis on AML12 cells overexpressing *Zac1*. (A) Venn diagram representing the number of DEGs after overexpression of *Zac1* (DEGs defined by $q < 0.05$ comparing *Zac1* to *EGFP*-overexpressing cells; $n = 3$ replicates) and their intersection with the IGN. Only IGN genes detected in RNA-seq are considered. Overrepresentation analysis was performed using a hypergeometric test. (B) Volcano plot of 13,800 genes identified through RNA-seq. The 733 DEGs are represented with dark gray dots. The DEGs identified as IGN members are indicated by bold black dots

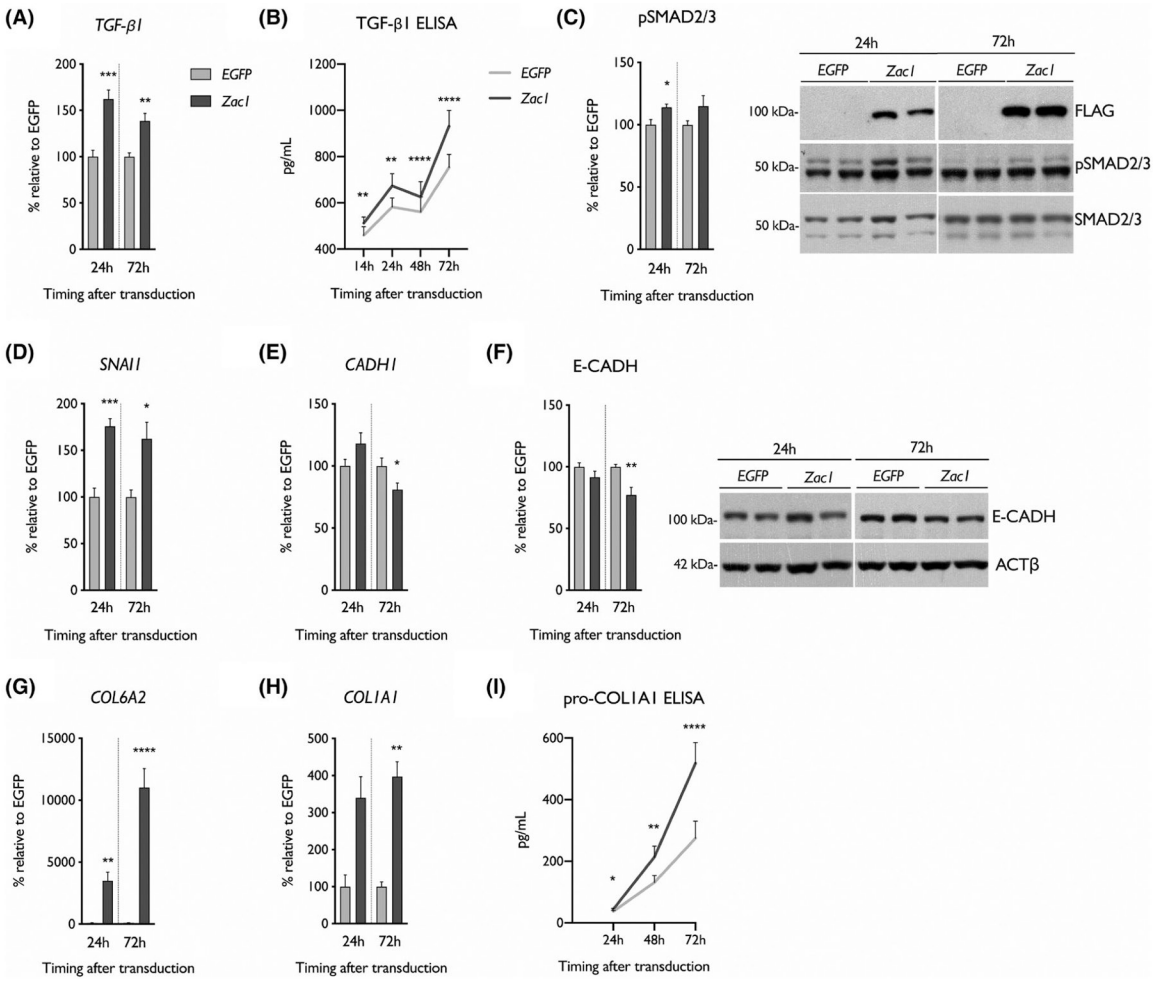

FIGURE 6.

Activation of TGF-β1 signaling in HepG2 cells overexpressing *Zac1*. (A) *TGF-β1* transcript accumulation at 24 h and 72 h after transduction with *EGFP* or *Zac1* overexpression constructs. (B) TGF-β1 concentration in the media of transduced cells. (C) Protein levels of Zac1-FLAG, P-SMAD2/3 (mothers against decapentaplegic homolog 2/3), and SMAD2/3 at 24 h and 72 h after transduction. Digital quantification of phospho-SMAD2/3 relative to SMAD2/3 (*left*). Representative immunoblot (*right*). (D,E) *SNAI1* (D) and *CADH1* (E) transcript accumulation 24 h and 72 h after transduction. (F) Protein levels of E-CADH and ACTB after transduction. Digital quantification of E-CADH relative to ACTB (*left*). Representative immunoblot (*right*). (G,H) *COL6A2* (G) and *COL1A1* (H) transcript accumulation 24 h and 72 h after transduction. (I) Pro-COL1A1 concentration in the media of transduced cells. Three independent experiments with $n = 3$ replicates/condition were performed. Data are presented as means ± SEM. $*p < 0.05$, $**p < 0.01$, $***p < 0.001$. Student's *t* test, two-tailed, comparing *Zac1* to *EGFP* overexpressing cells within the same timepoint. SNAI1, snail family transcriptional repressor 1.

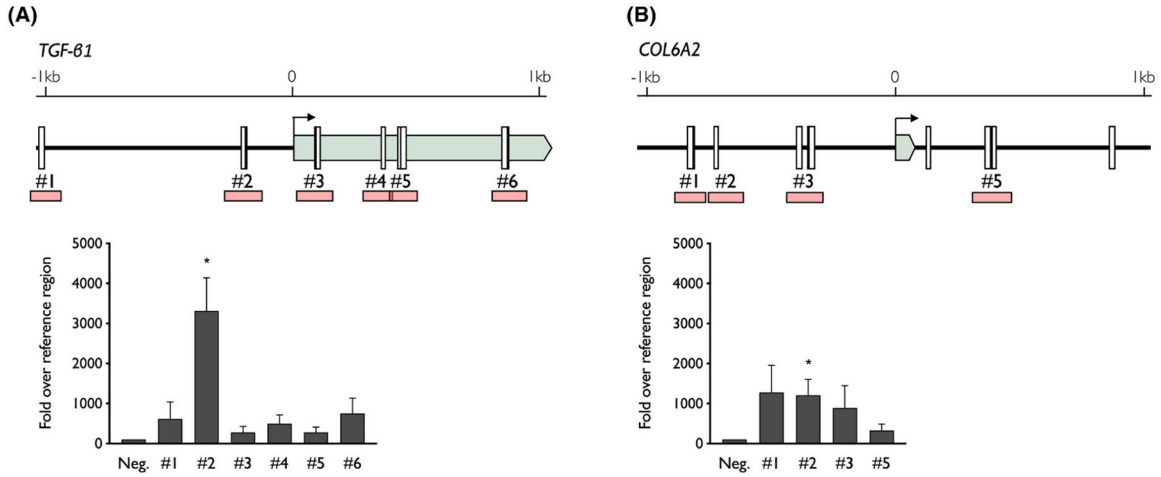

FIGURE 7.

Zac1 binding at the promoters of *TGF-β1* and *COL6A2*. Chromatin immunoprecipitation for Zac1-FLAG followed by quantitative PCR across computationally predicted Zac1 binding sites within 1 kb of the *TGF-β1* (A) and *COL6A2* (B) promoters. *Top:* Locus diagrams. For each locus, the green box indicates exon 1 with the direction of transcription shown. Arrows indicate the TSS. Vertical white bars indicate predicted Zac1 binding sites. Pink horizontal bars indicate the position of quantitative PCR assays. *Bottom:* Enrichment of Zac1-FLAG relative to control sequences at each of the amplified DNA regions shown above. Three independent experiments, each from a pool representative of $n = 6$ replicates, were performed. Data are presented as means ± SEM. $*p < 0.05$. Student's t test, two-tailed, comparing each amplicon to the negative control region

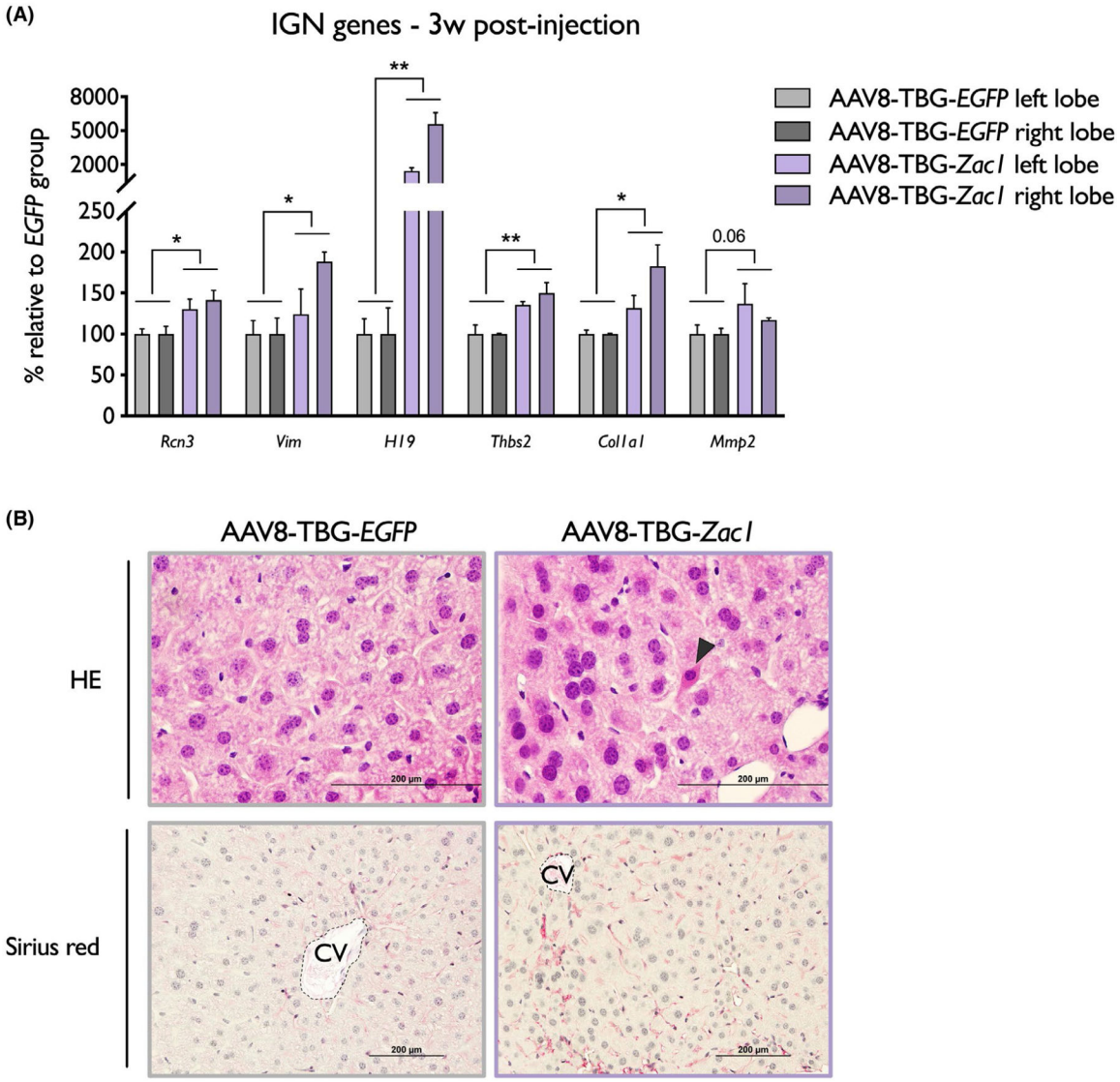

FIGURE 8.

Zac1 overexpression in hepatocytes in vivo. (A) IGN transcript accumulation in livers from females 3 weeks following injection. Two lobes are analyzed for each individual. Data are presented as means ± SEM. *$p < 0.05$, **$p < 0.01$. Nested Student's t test, two-tailed, comparing AAV8-TBG-*Zac1* to AAV8-TBG-*EGFP*. (B) Representative photomicrographs (magnification ×20) of liver sections from females 10 weeks following injection. Top row: H&E staining; arrowhead indicates apoptotic hepatocyte. Second row: sirius red staining. CV, central vein; EGFP, enhanced green fluorescent protein